

ARTICLE TYPE

High Energy Processes in Wolf-Rayet Stars

Stephen L. Skinner^{*1} | Werner Schmutz² | Manuel Güdel³ | Svetozar Zhekov⁴¹CASA, Univ. of Colorado, Boulder, CO 80309-0389, USA²PMOD, WRC, Davos Dorf, Switzerland³Dept. of Astrophysics, Univ. of Vienna, Vienna, Austria⁴Inst. of Astron. & Natl. Astron. Obs., Bulgarian Acad. Sci., Sofia, Bulgaria

Correspondence

^{*}Email: stephen.skinner@colorado.edu

Wolf-Rayet (WR) stars are massive ($\geq 10 M_{\odot}$) evolved stars undergoing advanced nuclear burning in their cores, rapidly approaching the end of their lives as supernovae. Their powerful winds enrich the interstellar medium with heavy elements, providing raw material for future generations of stars. We briefly summarize high-energy processes in WR stars, focusing mainly on their X-ray emission. We present new results from *Chandra* observations of the eclipsing WR+O binary CQ Cep covering a full orbit which stringently test X-ray emission models.

KEYWORDS:

stars: Wolf-Rayet; stars: individual (CQ Cep); X-rays: stars

1 | WOLF-RAYET STARS: OVERVIEW

WR stars are broadly classified into three subtypes based on their optical spectra: nitrogen-type (WN), carbon-type (WC), and oxygen-type (WO). WO stars are the most evolved and only a few are known in the Galaxy. WR stars have high effective temperatures $>20,000$ K and tremendous winds with typical mass-loss rates $\dot{M} \sim 10^{-5} M_{\odot} \text{ yr}^{-1}$. Terminal wind speeds for WN and WC stars are typically $V_{\infty} \sim 1000 - 2500 \text{ km s}^{-1}$, and even higher for WO stars. Most, but not all, WR stars are strong X-ray sources. Their X-ray emission is usually attributed to shocks associated with their supersonic winds, but shock model predictions are in some cases not compatible with the observed X-ray properties. Nonthermal (synchrotron) radio continuum emission has been detected in some WR binaries. WR binaries are potential sources of γ -ray emission and sites for Galactic cosmic ray acceleration.

2 | X-RAYS

2.1 | Single WR Stars

X-rays have been detected from putatively single (non-binary) WN and WO stars, but surprisingly not from WC stars. X-ray luminosities of WN stars span a range of about two orders of

magnitude with typical values $\log L_x \sim 10^{32 \pm 1} \text{ ergs s}^{-1}$ (Skinner et al. 2012). The only galactic WO star detected so far in X-rays is WR 142 with $\log L_x \approx 31.3 \text{ ergs s}^{-1}$ at its *GAIA* DR2 distance of 1.74 kpc (Sokal et al. 2010; Skinner et al. 2018). WC stars are X-ray faint or X-ray quiet for reasons not yet known, but strong wind absorption may be partially responsible. The most stringent upper limit obtained for a single WC star so far is from a *Chandra* observation of WR 135 (WC8) which gives $\log L_x \leq 29.99 \text{ ergs s}^{-1}$ at its *GAIA* DR2 distance of 2.11 kpc (Skinner et al. 2006).

The X-ray spectra of single WN stars can be acceptably modeled as a two-temperature (2T) optically-thin plasma with a cool component at $kT_1 \approx 0.3 - 0.7 \text{ keV}$ [$T_1 \approx 3 - 8 \text{ MK}$] and a hotter component at $kT_2 \approx 2 - 5 \text{ keV}$ [$T_2 \approx 20 - 60 \text{ MK}$] (Skinner et al. 2010; 2012). Such 2T models do not fully reflect the true physical conditions since the X-ray plasma is distributed over a range of temperatures.

The temperature of the cool component is consistent with predictions of radiative wind shock models, which posit X-ray production from shocks that form in the wind as a result of line-driven instabilities (e.g. Lucy & White 1980). Such models have had success in explaining the soft X-ray emission of some O-type stars, but their relevance to WR stars with much higher mass-loss rates and wind speeds remains to be determined. But the hotter plasma, which is prominent in single WN star spectra and in the spectrum of the WO star WR 142, is not anticipated from radiative shock models. Its origin is so far unexplained.

2.2 | WR Binaries

Massive WR binaries are typically strong X-ray sources. This includes WC systems such as γ^2 Vel (= WR 11; WC8+O7) and WN systems such as WR 147 (WN8+B0.5V). In some cases, the X-ray emission is bright enough to obtain high-resolution X-ray grating spectra, allowing individual emission lines to be identified and studied (e.g. γ^2 Vel, Skinner et al. 2001; WR 140, Pollock et al. 2005; WR48a, Zhekov et al. 2014). Line information, when available, constrains the plasma temperature distribution, metal abundances, and distance from the star(s) where the line forms.

The X-ray emission of WR binaries is potentially an admixture of multiple components including that of the individual stars (and their winds) and colliding wind (CW) shock emission originating between the stars, or near the surface of the star with the weaker wind (Usov 1992). In most cases, these different components cannot be spatially-resolved with current generation X-ray telescopes.

The maximum CW shock temperature for an adiabatic shock is $kT_{cw} \approx 1.96\mu[V_{\perp}/1000 \text{ km/s}]^2 \text{ keV}$. Here, μ is the mean atomic weight (amu) in the wind ($\mu \approx 4/3$ for He-dominated WN winds) and V_{\perp} is the wind velocity component perpendicular to the shock front. The hottest plasma is predicted to lie on or near the line-of-centers where $V_{\perp} \approx V_{\infty}$, if the winds have reached terminal speeds. This latter condition will be satisfied in wide binaries ($P_{orb} \sim \text{years}$) but not in close binaries ($P_{orb} \sim \text{days}$). For typical WR wind speeds $V_{\infty} \approx 1000 - 2500 \text{ km/s}$, maximum shock temperatures $kT_{cw,max} \approx 2 - 12 \text{ keV}$ are expected. Temperatures in this range are indeed observed in some WR binaries, but also in some (apparently) single WR stars.

3 | THE ECLIPSING WR BINARY CQ CEP

CQ Cep (= WR 155) is an eclipsing WN6+O9 binary system in a near-circular high inclination 1.64 d orbit (Demircan et al. 1997). The masses and radii of the two stars are nearly equal ($M_* \approx 21 M_{\odot}$, $R_* \approx 8 R_{\odot}$). Their separation is $D \approx 20 R_{\odot}$, placing the two stars nearly in contact (Demircan et al. 1997). At such close separation, the winds will not have reached terminal speeds before colliding. The higher momentum of the WR wind will overpower the O star wind and the CW shock will form at or near the O star surface. CQ Cep is a superb system for testing CW model predictions at close spacing where the winds will be at subterminal speeds and radiative cooling may be important (Stevens et al. 1992).

We have observed CQ Cep with the *Chandra* X-ray Observatory using the ACIS-S CCD imaging spectrometer over a full orbit (Table 1). The first half of the orbit was observed in a single uninterrupted observation in March 2013, capturing the

TABLE 1 Chandra Observations of CQ Cep

ObsId	Start Date	Duration (ks)	Phase (ϕ)	Rate (c ks ⁻¹)	P _{var}
14538	2013 Mar 19	85.6	(−0.10, 0.50)	24.7±5.6†	0.22
17734	2017 Feb 27	18.3	(−0.07, 0.06)	20.9±4.0	0.16
20016	2017 Mar 4	16.4	(0.66, 0.78)	20.3±3.9	0.07
20017	2017 Mar 5	33.9	(0.43, 0.67)	20.5±4.1	0.05
20018	2017 Mar 5	19.2	(0.79, 0.93)	20.6±4.7	0.04

O star is in front at $\phi = 0$. P_{var} is the probability of variable count rate based on the *Chandra* *glvary* statistical test.

†ACIS-S effective area was higher in 2013.

O star passing in front of the WR star at $\phi = 0$ (Skinner et al. 2015). The second half was observed in four exposures during Feb.-March 2017, again capturing the O star in front as well as the WR star in front. Simultaneous optical light curves were obtained using the *Chandra* Aspect Camera Assembly (ACA). The main objective was to search for X-ray variability during eclipses, which is expected if the hottest X-ray plasma is confined to the region on or near the line-of-centers between the two stars.

Both the primary and secondary visual eclipses are clearly seen in the optical light curves (Fig. 1-top panels). Comparison of the overlapping ACA light curves indicates that the system was slightly brighter in 2013 than in 2017. Optical variability is also apparent from significant scatter in the high-precision *GAIA* photometry at similar phases but different epochs. The times of minimum ACA optical brightness at $\phi=0$ in 2013 and 2017 give an accurate orbital period $P = 1.641239 (\pm 8.0e-07)$ d. Analysis of historical data suggests that the period may be variable (Koenigsberger et al. 2017).

In contrast, the phased X-ray light curves (Fig. 1-bottom panels) show only low-level fluctuations. No statistically significant variability is present and the mean count rates of the observations agree to within $\pm 1\sigma$ (Table 1). ACIS-S effective area declined during 2013-2017 due to contaminant buildup, resulting in lower count rates in 2017.

Phase-resolved X-ray spectra obtained in 2017 are shown in Figure 2-top. All four spectra are similar and spectral fits show no significant difference in their observed X-ray fluxes. The median energies of the photons detected in the observations are nearly identical, i.e. $E_{50} = 1.88, 1.90, 1.87, \text{ and } 1.87 \text{ keV}$ (background is negligible). The spectra are overlaid in Figure 2-bottom. Several blended emission lines are detected including Ne X, Mg XI, Si XIII, S XV, Ar XVII and possibly Ne IX and Ca XIX. Faint Fe K (Fe XXV) emission was detected in the 2013 observation (Skinner et al. 2015), tracing very hot plasma at $T \sim 63 \text{ MK}$.

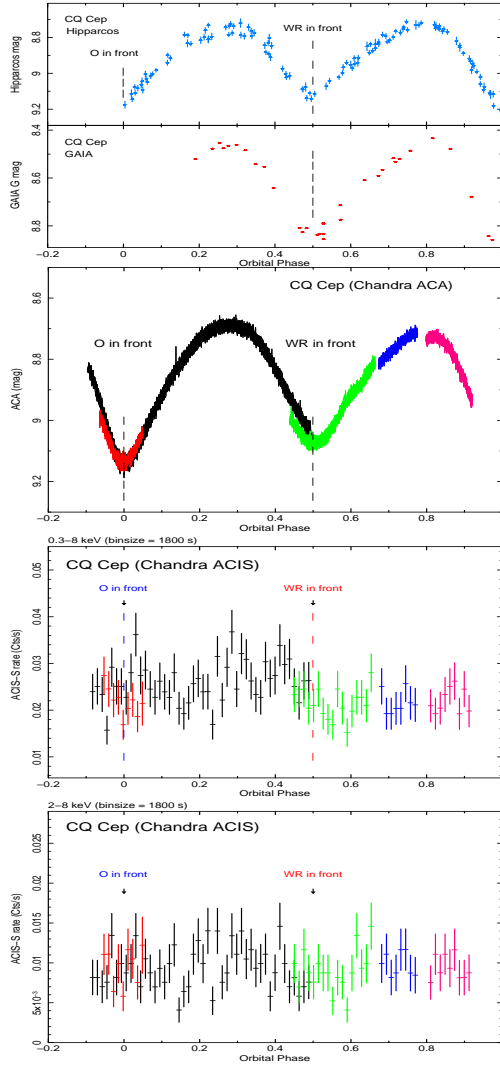


FIGURE 1 Phased CQ Cep light curves. Top: Optical (Hipparcos epoch 1990.0-1993.1, GAIA G mag epoch 2013.3-2014.6; 1σ errors). 2nd row: Optical (Chandra ACA), color coded by observation date (Table 1). 3rd row: Chandra X-ray broad (0.3-8 keV). Bottom: Chandra X-ray hard (2-8 keV).

Spectral fits with non-solar abundance 2T models are able to reproduce the spectra. The inferred absorption (N_H) and plasma temperatures (kT) are somewhat model dependent, as is the intrinsic (unabsorbed) X-ray luminosity (L_x). Fits of the 2013 spectrum were discussed in Skinner et al. (2015). Table 2 compares fits of the 2013 and 2017 spectra using a 2T plane-parallel shock model. The temperature of the hot component ($kT_2 \approx 3.4$ -3.6 keV) is about twice the predicted value for the WN6 wind shocking onto the surface of the O star companion at subterminal speed (Skinner et al. 2015). However, the predicted shock temperature depends on the assumed WR wind acceleration profile in the region between the stars, which is not well-constrained observationally.

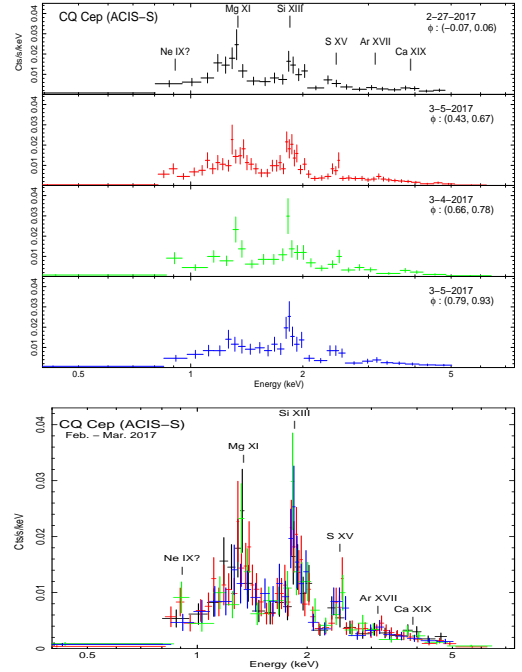


FIGURE 2 Chandra X-ray spectra of CQ Cep obtained in 2017. Top: Separated by observation (Table 1). Bottom: All four spectra overlaid.

The intrinsic (unabsorbed) X-ray luminosity of CQ Cep at its GAIA distance (Table 2) is at the high end of the range for WR stars. The predicted luminosity for a WR wind shocking onto the surface of an O-type companion of radius R at separation D is $L_{x,cw} = 0.125(R/D)^2 L_{wind,wr} F$. The WR wind kinetic luminosity is $L_{wind,wr} = (1/2)\dot{M}_{wr} V_{\infty,wr}^2$. The correction factor $F < 1$ accounts for changes in the direction and magnitude of the WR wind velocity vector across the O-star surface, which must be considered in closely-spaced binaries where the stellar radii are nearly equal, as in CQ Cep. Inserting appropriate values for CQ Cep, one obtains $\log L_{x,cw} = 35.11 - 35.27$ ergs s^{-1} (Skinner et al. 2015), which is about fifty times greater than observed. Similar discrepancies have been noted in other close WR binaries and explanations involving inhomogeneous winds have been proposed (Zhekov 2012).

The absence of significant X-ray variability during eclipses is remarkable in comparison to the dramatic optical variability. This lack of variability, even in the high 2-8 keV energy range, indicates that the hottest X-ray plasma occupies a region much larger than the scale of the binary system and is not localized near the line-of-centers. If the hot plasma does form in a CW shock, then orbital motion may have distorted the shape of the interaction region and displaced it away from the line-of-centers (Skinner et al. 2015, and references therein).

TABLE 2 CQ Cep Spectral Fits (shock model)

Year	$N_{H,1}, N_{H,2}$ (10^{21} cm^{-2})	kT_1, kT_2 (keV)	F_x^\dagger	$\log L_x^\ddagger$ (erg s^{-1})
2013	4.4[1.7], 0.3[0.1]	0.6[0.1], 3.4[0.6]	2.09	33.43
2017	6.5[2.7], 0.3[0.1]	1.0[0.3], 3.6[0.9]	2.20	33.53

Fits are based on a 2T plane-parallel shock model (XSPEC *vphshock*). The 2017 values are from a simultaneous fit of all 4 spectra. The absorption N_H of each temperature component was allowed to vary independently. The tabulated N_H values do not include interstellar absorption, held fixed at $N_H = 4.4 \times 10^{21} \text{ cm}^{-2}$. Solar abundances were used for the cool component and generic WN abundances for the hot component (Skinner et al. 2015). Brackets enclose 1σ errors.

† Absorbed flux (0.3–8 keV). Units: $10^{-13} \text{ ergs cm}^{-2} \text{ s}^{-1}$.

‡ Unabsorbed X-ray luminosity ($d=3.32 \text{ kpc}$; GAIA DR2).

4 | NONTHERMAL RADIO EMISSION

Thermal (free-free) radio continuum emission is produced by the strong photoionized winds of WR stars. In addition, radio continuum emission characterized by negative or flat spectral indices $\alpha \leq 0$ (flux density varies with frequency as $F_\nu \propto \nu^\alpha$) interpreted as synchrotron emission has been detected in several WR+OB binaries (Abbott et al. 1986). It is believed that the nonthermal radio emission is produced in the CW region between the stars where electrons are accelerated to relativistic energies by shocks, but magnetic fields may also play a role (Kissmann et al. 2016). Support for the origin of nonthermal radio emission in the CW region comes from spatially-resolved radio observations of WR 147 (Churchwell et al. 1992). The detectability of any nonthermal radio emission is affected by absorption and viewing geometry. As a result, nonthermal emission is not seen in all WR binaries.

5 | GAMMA-RAYS

The formation of a WR+BH binary may be accompanied by a γ -ray burst (Tutukov & Cherepashchuk 2003). The best candidate for a WR+BH system to date is Cyg X-3 (Schmutz et al. 1996). Some models predict that electrons in the CW region of WR binaries will be accelerated up to γ -ray energies by shocks and inverse Compton scattering (e.g. Benaglia & Romero 2003). Initial support for this idea comes from the reported *Fermi*-LAT γ -ray detection of the WR binary γ^2 Vel by Pshirkov (2016). Although this report is encouraging, the detection significance (6σ) is relatively low and other WR binaries in the Pshirkov (2016) sample were undetected by *Fermi*. Improvements in the sensitivity and angular resolution

of γ -ray telescopes will be needed to quantify the properties of WR binaries in this very high energy ($\sim 1 - 100 \text{ GeV}$) regime.

6 | CONCLUSIONS

Wolf-Rayet stars exhibit a diverse range of high-energy phenomena, largely attributed to their powerful shocked winds. But details of the underlying emission mechanisms are still not well-understood. Hot X-ray plasma is prevalent in WN and WO stars but temperatures and luminosities are not fully in accord with shock model predictions. Other factors such as magnetic fields may be involved in WR X-ray production. Mysteriously, carbon-rich WC stars remain undetected in X-rays. Nonthermal (synchrotron) radio emission has been traced to the colliding wind region in WR binaries, but the mechanism(s) which accelerate electrons to relativistic energies is still debated. Gamma-ray emission has been reported from the nearest WR binary γ^2 Vel. Future improvements in sensitivity and angular resolution will be needed to confirm this intriguing discovery and search for γ -rays in more distant WR systems.

ACKNOWLEDGMENTS

This work was supported by SAO/CXC award GO6-17009X.

REFERENCES

- Abbott, D. e. a. 1986, *ApJ*, 303, 239.
 Benaglia, P., & Romero, G. 2003, *A&A*, 399, 1121.
 Churchwell, E. e. a. 1992, *ApJ*, 393, 329.
 Demircan, O. e. a. 1997, *AN*, 318, 267.
 Kissmann, R. e. a. 2016, *ApJ*, 831, 121.
 Koenigsberger, G. e. a. 2017, *A&A*, 601, A121.
 Lucy, L., & White, R. 1980, *ApJ*, 241, 300.
 Pollock, A. e. a. 2005, *ApJ*, 629, 482.
 Pshirkov, M. 2016, *MNRAS*, 457, 99.
 Schmutz, W. e. a. 1996, *A&A*, 311, L25.
 Skinner, S. e. a. 2006, *Ap&SS*, 304, 97.
 Skinner, S. e. a. 2010, *AJ*, 139, 825.
 Skinner, S. e. a. 2012, *AJ*, 143, 116.
 Skinner, S. e. a. 2015, *ApJ*, 799, 124.
 Skinner, S. e. a. 2018, *ApJ*, in press.
 Sokal, K. e. a. 2010, *ApJ*, 715, 1327.
 Stevens, I. e. a. 1992, *ApJ*, 386, 265.
 Tutukov, A., & Cherepashchuk, A. 2003, *Ast. Rep.*, 47, 386.
 Usov, V. 1992, *ApJ*, 389, 635.
 Zhekov, S. 2012, *MNRAS*, 422, 1332.
 Zhekov, S. e. a. 2014, *ApJ*, 785, 8.

